Eur. Phys. J. C (2025) 85:661
https://doi.org/10.1140/epjc/s10052-025-14389-2

THE EUROPEAN PHYSICAL JOURNAL C

Regular Article - Theoretical Physics

Thermodynamic topology of AdS black holes in rainbow gravity

Ping Yin, Yaqin Liu, Juhua Chen[a], Yongjiu Wang

Department of Physics, Key Laboratory of Low Dimensional Quantum Structures and Quantum Control of Ministry of Education, and Synergetic Innovation Center for Quantum Effects and Applications, Hunan Normal University, Changsha 410081, Hunan, People's Republic of China

Received: 24 April 2025 / Accepted: 31 May 2025

Abstract In this paper, we study the topology of four-dimensional AdS black holes with nonlinear sources in the framework of rainbow gravity. We apply the Duan's φ-mapping theory and the method of generalized free energy to study the topological charges related to critical points and the local and global topology at black hole thermodynamic defects, respectively. By analyzing the critical points of black holes in the canonical ensemble (CE) and the grand canonical ensemble (GCE), we find the nonlinear parameter p does not affect the total topological number of black holes, which always remains $+1$, but there is one novel critical point appearing in GCE. And we also find the topological number of black hole is $+1$ in CE, while in GCE, the topological number can be 0 or $+1$, depending on the system pressure and the electric potential, respectively. Our results show that the topological classification of AdS black holes depends significantly on the ensemble selection, and the rainbow gravity effect has no effect on its topological number.

1 Introduction

Black holes, mysterious entities at the intersection of gravity and quantum mechanics, have captured the keen interest of scientists since the early 20th century. Notably, in the early 1970s, Stephen Hawking et al. first proposed the concept that black holes possess temperature and entropy. This revolutionary discovery prompted a reexamination of the nature of black holes within the scientific community [1–10]. The laws of black hole mechanics, proposed by Bardeen et al., laid a solid foundation for the development of black hole thermodynamics and resonated with the law of conservation of energy in the second law of thermodynamics [11]. Black hole thermodynamics has not only deepened the understanding of black holes, but also facilitated the cross-disciplinary integration of general relativity, quantum mechanics and statistical physics, propelling the advancement of these fields. In the context of Anti-de Sitter (AdS) spacetime, black holes are of particular interest due to their critical role in the AdS/CFT correspondence. This correspondence reveals a profound duality between gravitational theories in AdS space and conformal field theories on its boundary [12]. Research into the thermodynamic properties of AdS black holes has demonstrated the existence of a phase transition between stable large black holes in AdS spacetime, known as the Hawking-Page phase transition [13], which can be interpreted as a confinement/deconfinement phase transition in gauge theory [14]. Additionally, for charged black holes, a first-order phase transition similar to the liquid–gas phase transition in Van der Waals fluids has been observed [15,16]. These findings not only enrich our understanding of the thermodynamic properties of AdS black holes, but also provide a new perspective for comprehending the connection between black holes and quantum field theories. Within the framework of the extended phase space, the thermodynamic phase transition properties of AdS black holes have been extensively studied [17–29]. The cosmological constant is treated as a dynamic variable and is endowed with the physical significance of pressure. Concurrently, the mass of the black hole is no longer simply regarded as internal energy but is redefined as enthalpy. This transformation of the theoretical framework enables the observation of a richer array of phenomena, such as reentrant phase transitions, triple points, and polymer-like phase transitions.

To address the discrepancies between the two fundamental pillars of modern physics, General Relativity and Quantum Mechanics, scientists have proposed several theoretical models: loop quantum gravity [30], string theory [31], and spacetime foam models [32]. In these models, the Planck length is considered as the smallest observable length scale. The existence of this minimum observable length scale challenges certain assumptions of Special Relativity [33–38]. Lorentz

[a] e-mail: jhchen@hunnu.edu.cn (corresponding author)

Published online: 15 June 2025

invariance is a fundamental requirement of both relativity and quantum field theory, and is consistent with the continuity of spacetime at any scale. Theoretically, the scale of any object can be made infinitely small through Lorentz transformations, which contradicts the concept of the minimum length unit in quantum gravity. To resolve this contradiction, scientists have proposed a theory that modifies the Lorentz transformations, known as Doubly-Special Relativity (DSR) [39–42]. The core idea of this theory is to introduce two natural constants, the Planck energy constant and the speed of light, to replace a single constant, thereby maintaining the consistency of the theory at high-energy limits [43]. Within the framework of DSR, the dispersion relation is expressed as $E^2 f_\varepsilon - p^2 g_\varepsilon = m^2$, where f_ε and g_ε are commonly regarded as rainbow functions, motivated by phenomenological considerations [44], and $\varepsilon = \frac{E}{E_p}$, with E_p representing the Planck energy and E denoting the energy of the particle. Next, Magueijo and Smolin proposed extending DSR to curved spacetime [45], suggesting that the geometric shape of spacetime depends on the energy of the probing particle, the concept known as rainbow gravity, thereby introducing a series of energy-dependent metrics, i.e. rainbow metrics [46]. In this paper, we are interested in studying AdS black holes with a nonlinear parameter in gravity's rainbow.

In the study of black hole thermodynamics, attention has been extended to the topological properties within the thermodynamic phase space of black holes. In Refs. [47,48], two distinct methods for studying the topological thermodynamics of black holes have been proposed by Wei et al.. The first involves utilizing Duan's topological current φ-mapping theory [49,50] to ascertain the temperature function and to formulate the potential function. The second method regards the black hole solution as topological defects in the corresponding thermodynamic space, and studies its solution and the stability of the black hole through generalized free energy. Wei's research also indicates that first-order phase transitions occur only at the conventional critical point (with topological charge of -1), not at the novel critical point (with topological charge of $+1$) [47]. Researchers have expanded the field of black hole thermodynamic topology to encompass various types of black holes and a range of gravitational models [51–71].

The layout of this paper is as follows: we briefly review the black hole topology in Sect. 2 and the thermodynamic properties of two types of four-dimensional AdS black holes with nonlinear parameters in the context of gravitational rainbow theory in Sect. 3. We explore the thermodynamic topology of black holes in canonical ensemble in Sect. 4 and grand canonical ensemble in Sect. 5. Finally, we summarize our results in Sect. 6. (The units in this paper are $c = G = \hbar = k_B = 1$)

2 Topology of Black Holes thermodynamics

In this section, we briefly review the method for studying topology as presented in Refs. [47,48]. Starting from the temperature function in the extended thermodynamic space, it can be expressed as a function of entropy S, pressure P, and other parameters x^i. Based on this method, the critical points of the black hole can be derived from the subsequent relationships

$$(\partial_S T)_{P,x^i} = 0, \quad \left(\partial_{S,S} T\right)_{P,x^i} = 0. \tag{1}$$

From Eq. (1), we obtain a new temperature function that does not include the thermodynamic pressure term. Consequently, the Duan's potential function can be formulated as follows [47]

$$\Phi = \frac{1}{\sin\theta} T\left(S, x^i\right), \tag{2}$$

where $\frac{1}{\sin\theta}$ is an auxiliary factor, aiming to simplify the complexity of topological studies.

We introduce a new vector field $\phi = (\phi^S, \phi^\theta)$

$$\phi^S = (\partial_S \Phi)_{\theta,x_i}, \phi^\theta = (\partial_\theta \Phi)_{S,x_i}. \tag{3}$$

The boundaries of the parameter space are defined by the horizontal lines $\theta = 0$ and $\theta = \pi$, while the zero points of the vector field are located at $\theta = \frac{\pi}{2}$. Within the framework of Duan's ϕ-mapping theory [49,50] the corresponding topological current can be expressed in the following form

$$J^\mu = \frac{1}{2\pi} \epsilon^{\mu\nu\lambda} \epsilon_{ab} \partial_\nu n^a \partial_\lambda n^b, \tag{4}$$

where ∂_ν denotes the partial derivative of x^ν, and $x^\nu = (t, r, \theta)$. The normalized vector n is defined as $n^a = \frac{\phi^a}{\|\phi\|}$ $(a = 1, 2)$, where $\phi^1 = \phi^S$ and $\phi^2 = \phi^\theta$. By combining the Jacobi tensor $\epsilon^{ab} J^\mu \left(\frac{\phi}{x}\right) = \epsilon^{\mu\nu\rho} \partial_\nu \phi^a \partial_\rho \phi^b$ and the two-dimensional Laplacian Green function $\Delta_{\phi^a} \ln ||\phi|| = 2\pi\delta(\phi)$, it can be concluded that topological current is non-zero only at the zero point of the vector field. Therefore, the topological charge corresponding to the parameter region can be calculated as follows

$$Q_t = \int_\Sigma j^0 d^2x = \sum_{i=1}^{N} w_i, \tag{5}$$

where j^0 represents the density of the topological current, while the parameter w_i denotes the winding number associated with the ith zero of the vector field. The total topological charge Q_t can be obtained by summing the winding numbers of each zero point. This method provides a comprehensive

understanding of the topology of black holes by summarizing the contributions of all individual critical points. The paper [48] shows the expression for the generalized free energy of any black hole as

$$\mathcal{F} = E - \frac{S}{\tau}, \tag{6}$$

where E and S represent the energy and entropy of a black hole, respectively, and τ is a time scale parameter that can be interpreted as the inverse of the equilibrium temperature of the cavity surrounding the black hole, i.e. $\tau = \frac{1}{T}$. To utilize the generalized free energy, the vector field ϕ can be defined as follows

$$\phi = \left(\frac{\partial \mathcal{F}}{\partial r_+}, -\cot\Theta \csc\Theta\right). \tag{7}$$

At $\Theta = \frac{\pi}{2}$, the zero points of the vector field ϕ can be identified, and the unit vector is defined by the following equation

$$n^a = \frac{\phi^a}{\|\phi\|} \quad (a = 1, 2) \quad \text{and} \quad \phi^1 = \phi^{r_+}, \quad \phi^2 = \phi^{\Theta}. \tag{8}$$

From the topological perspective, each black hole solution is endowed with a topological charge, which can be $+1$ or -1. Consequently, the total topology number of a black hole is obtained by aggregating the winding numbers of associated with each branch. That is

$$W = \sum_{i=1}^{N} \omega_i. \tag{9}$$

3 Thermodynamics of AdS Black Holes in rainbow gravity with nonlinear source

Within the framework of a four-dimensional AdS space-time, the action of nonlinear charged black holes in the context of Einstein-Λ gravity is [72]

$$I = -\frac{1}{16\pi}\int \sqrt{-g}[R - 2\Lambda + \mathcal{L}(\mathcal{F})]d^4x. \tag{10}$$

where the parameters R and Λ represent the $Ricci$ scalar and the cosmological constant, respectively. The last term is the electromagnetic Lagrangian density. In this context, the power-law nonlinear electrodynamics form is $\mathcal{L}(\mathcal{F}) = (-\mathcal{F})^p$ [73,74], which implies that the electromagnetic Lagrangian density can be treated as a power function of Maxwell's invariant. The Maxwell invariant, denoted as $\mathcal{F} = F^{\mu\nu}F_{\mu\nu}$, with $F_{\mu\nu} = \partial_\mu A_\nu - \partial_\nu A_\mu$, where A_μ is the gauge potential. This invariant plays a central role in the Lagrangian formulation of electromagnetic interactions.

By considering Eq. (10), the field equations related to gravity and gauge are

$$\begin{aligned} &R_{\mu\nu} - \frac{1}{2}Rg_{\mu\nu} + \Lambda g_{\mu\nu} = \frac{1}{2}g_{\mu\nu}(-\mathcal{F})^p \\ &\quad + 2p\,(-\mathcal{F})^{p-1}\,F_{\mu\alpha}F^{\alpha}_{\nu}, \\ &\partial_\mu\left[\sqrt{-g}\mathcal{L}'(\mathcal{F})F^{\mu\nu}\right] = 0. \end{aligned} \tag{11}$$

In four-dimensional AdS spacetime, the line element for a black hole in rainbow gravity is

$$ds^2 = -\frac{V(r)}{f_\varepsilon^2}dt^2 + \frac{1}{g_\varepsilon^2}\left[\frac{dr^2}{V(r)} + r^2(d\theta^2 + \sin^2\theta d\varphi^2)\right]. \tag{12}$$

Combining Eqs. (11) and (12), the different components of the gravitational field equations can be expressed as

$$e_{tt} = e_{rr} = \begin{cases} g_\varepsilon^2\left(V''(r) + \frac{2V'(r)}{r}\right) + 2\Lambda - 2\sqrt{2}\frac{q_\varepsilon^3}{r^3} = 0 & \text{for} \quad p = \frac{3}{2}, \\ g_\varepsilon^2\left(V''(r) + \frac{2V'(r)}{r}\right) + 2\Lambda - 2^p q_\varepsilon^{2p} r^{-\frac{4p}{2p-1}} = 0 & \text{for} \quad \frac{1}{2} < p < \frac{3}{2}, \end{cases} \tag{13}$$

$$e_{\theta\theta} = e_{\varphi\varphi} = \begin{cases} 2g_\varepsilon^2\left(\frac{V'(r)}{r} + \frac{V'(r)-1}{r^2}\right) + 2\Lambda + 4\sqrt{2}\frac{q_\varepsilon^3}{r^3} = 0 & \text{for} \quad p = \frac{3}{2}, \\ 2g_\varepsilon^2\left(\frac{V'(r)}{r} + \frac{V'(r)-1}{r^2}\right) + 2\Lambda + (2p-1)2^p q_\varepsilon^{2p} r^{-\frac{4p}{2p-1}} = 0 & \text{for} \quad \frac{1}{2} < p < \frac{3}{2}. \end{cases} \tag{14}$$

Therefore, the metric function in the above equation is

$$V(r) = \begin{cases} 1 - \frac{m}{r} - \frac{\Lambda r^2}{3g_\varepsilon^2} - \frac{2\sqrt{2}q_\varepsilon^3}{rg_\varepsilon^2}\ln\left(\frac{r}{\ell}\right) & \text{for} \quad p = \frac{3}{2}, \\ 1 - \frac{m}{r} - \frac{\Lambda r^2}{3g_\varepsilon^2} - \frac{(2p-1)^2(2)^{p-1}q_\varepsilon^{2p}}{(2p-3)g_\varepsilon^2} r^{\frac{-2}{2p-1}} & \text{for} \quad \frac{1}{2} < p < \frac{3}{2}. \end{cases} \tag{15}$$

where m and q_ε are mass parameter and charge of black hole. f_ε and g_ε are rainbow function parameters. The metric function for the case $p = 1$ corresponds to the Reissner–Nordström (R–N) AdS black hole in the context of gravity's rainbow [44].

In the expanded phase space, the expression for the cosmological constant and thermodynamic pressure is $P = -\frac{\Lambda}{8\pi}$

[75–77]. Based on the above premises, the Hawking temperature T, mass M, entropy S, and electric charge Q of a black hole expressed in terms of the horizon radius r_+ are given by

$$M = \frac{m}{2f_\varepsilon g_\varepsilon} = \frac{1}{2f_\varepsilon g_\varepsilon} \begin{cases} \frac{3g_\varepsilon^2 r_+ + 8P\pi r_+^3 - 6\sqrt{2}q_\varepsilon^3 \ln(\frac{r_+}{\ell})}{3g_\varepsilon^2} & \text{for} \quad p = \frac{3}{2}, \\ r_+ + \frac{2^{p-1}(2p-1)^2 q_\varepsilon^{2p} r_+^{1-\frac{2}{2p-1}}}{g_\varepsilon^2(2p-3)} - \frac{8P\pi r_+^3}{3g_\varepsilon^2} & \text{for} \quad \frac{1}{2} < p < \frac{3}{2}, \end{cases} \tag{16}$$

$$T = \frac{\kappa}{2\pi} = \frac{g_\varepsilon}{4\pi f_\varepsilon}\frac{d}{dr}V(r)|_{r=r_+} = \frac{g_\varepsilon}{4\pi f_\varepsilon r_+} \begin{cases} 1 + \frac{8P\pi r_+^2}{g_\varepsilon^2} - \frac{2\sqrt{2}q_\varepsilon^3}{g_\varepsilon^2 r_+} & \text{for} \quad p = \frac{3}{2}, \\ 1 + \frac{8P\pi r_+^2}{g_\varepsilon^2} - \frac{2p-1}{g_\varepsilon^2}\frac{2^{p-1}q_\varepsilon^{2p}}{r_+^{2p-1}} & \text{for} \quad \frac{1}{2} < p < \frac{3}{2}, \end{cases} \tag{17}$$

$$S = \frac{A}{4} = \frac{\pi r_+^2}{g_\varepsilon^2}, \tag{18}$$

$$Q = \begin{cases} \frac{3}{\sqrt{2}g_\varepsilon^2}q_\varepsilon^2 & \text{for} \quad p = \frac{3}{2}, \\ \frac{p2^{p-1}}{g_\varepsilon^2}q_\varepsilon^{2p-1} & \text{for} \quad \frac{1}{2} < p < \frac{3}{2}. \end{cases} \tag{19}$$

The first law of thermodynamics of the AdS black hole is

$$dM = TdS + UdQ, \tag{20}$$

where $T = \left(\frac{\partial M}{\partial S}\right)_Q$ and $U = \left(\frac{\partial M}{\partial Q}\right)_S$.

4 AdS black holes in rainbow gravity with nonlinear source in canonical ensemble

In this section, we mainly study the topology of AdS black holes under the rainbow gravity in canonical ensemble and for two cases in different region p.

4.1 Case 1: $p = \frac{3}{2}$

According the method mentioned in Sect. 2, the Hawking temperature is expressed as a function of charge through Eqs. (1) and (17)

$$T = \frac{g_\varepsilon(-2 \times 2^{1/4}\sqrt{3}g_\varepsilon Q^{3/2} + 3r_+)}{6f_\varepsilon \pi r_+^2}. \tag{21}$$

The potential function Φ under this condition is

$$\Phi = \frac{g_\varepsilon(2 \times 2^{1/4}\sqrt{3}g_\varepsilon Q^{3/2} - 3r_+)\csc\theta}{6f_\varepsilon \pi {r_+}^2}. \tag{22}$$

The vector field $\phi = \left(\phi^{r_+}, \phi^\theta\right)$ contains the following components

$$\begin{aligned} \phi^{r_+} &= \frac{g_\varepsilon(4 \times 2^{1/4}\sqrt{3}g_\varepsilon Q^{3/2} - 3r_+)\csc\theta}{6f_\varepsilon \pi r_+^3}, \\ \phi^\theta &= \frac{g_\varepsilon(2 \times 2^{1/4}\sqrt{3}g_\varepsilon Q^{3/2} - 3r_+)\cot\theta\csc\theta}{6f_\varepsilon \pi r_+^2}. \end{aligned} \tag{23}$$

According to Eq. (23), we can obtain the normalized vector $n = (\frac{\phi^{r_+}}{\|\phi\|}, \frac{\phi^\theta}{\|\phi\|})$. In Fig. 1a, we identify the emergence of a critical point CP_1 $(3.02099, \pi/2)$, which represents the end point of the first-order phase transition.

From the topological standpoint, we can find that the topological charge is non-zero when a critical point is enclosed by a contour. Conversely, the topological charge is zero. Therefore, we can determine the value of topological charge corresponding to the critical point which is surrounded by the contour C_1 or C_2. The contour can be parameterized as

$$\begin{cases} r = a\cos\vartheta + r_0, \\ \theta = b\sin\vartheta + \frac{\pi}{2}, \end{cases} \tag{24}$$

where r_0 represents an arbitrary length scale determined by the size of the cavity surrounding the black hole. For the contours C_1 and C_2, we set the values of the parameters as $(a, b, r_0) = (0.5, 0.2, 3.02099)$ and $(0.5, 0.3, 4.1)$, respectively. Since the given parameters alone cannot directly determine the topological charge of the black hole, the physical quantity of the deflection angle of the vector ϕ is introduced. For deflection along the given contours are

$$\Omega(\vartheta) = \int_0^\vartheta \epsilon_{ab} n^a \partial_\vartheta n^b d\vartheta. \tag{25}$$

When $\vartheta = 2\pi$, the topological charge of the corresponding critical points can be obtained by $Q = \frac{\Omega(2\pi)}{2\pi}$. The topological charge is -1 for the the critical point CP_1 surrounded by C_1 with the red solid line in Fig. 1b. The topological charge corresponding to the blue dashed line C_2 is zero, as no critical points can be found in the range surrounded the contour. Therefore, the topological charge Q_{CP_1} is -1. Furthermore, based to equation of state (17), we can obtain the corresponding critical point quantities as

$$r_c = \frac{4 \times 2^{1/4}g_\varepsilon - Q^{3/2}}{\sqrt{3}}; \quad P_c = \frac{1}{128\sqrt{2}\pi Q^3}; \quad T_c = \frac{\sqrt{3}}{16 \times 2^{1/4} f_\varepsilon \pi Q^{3/2}}. \tag{26}$$

In the four-dimensional AdS space-time, we can know that the critical point obtained from the thermodynamic topology exactly corresponds to the critical radius from the Eq. (26). Next, we plot the isobaric curves around the critical point

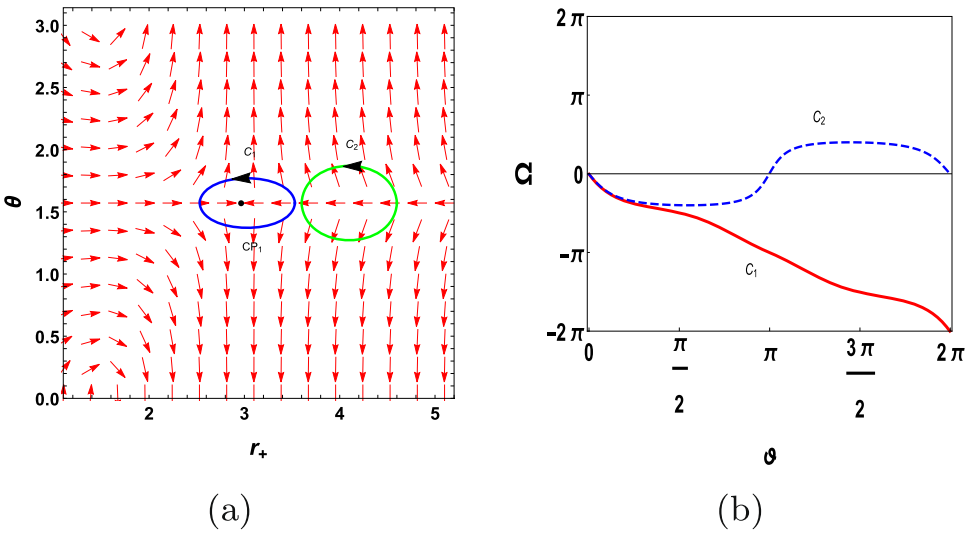

Fig. 1 **a** Shows the normalized vector field n in the r_+ vs θ plane and the critical point indicated by a black dot in canonical ensemble for $p = \frac{3}{2}$. **b** Shows the deflection angle of normalized vector field n in Ω vs ϑ plane for the contour C_1 and C_2. (By fixed $Q = 1$, $f_\varepsilon = 1.1$ and $g_\varepsilon = 1.1$)

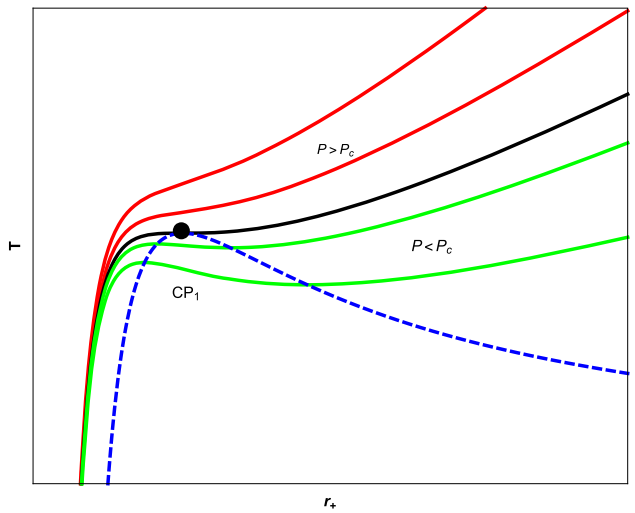

Fig. 2 Isobaric curves of AdS black hole in canonical ensemble for $p = \frac{3}{2}$. Black dot represents the critical point

CP_1 to study the characteristics of the critical point. The isobaric curves are shown in Fig. 2, where the black curve represents $P = P_c$, and the red and green curves correspond to the regions where $P > P_c$ and $P < P_c$, respectively. The unstable region for $P < P_c$ can be categorized into small and large black hole phases. Additionally, according to the blue curve described by the Eq. (21), we can identify the critical points. The phase of black hole always converges at the critical point, so the critical point CP_1 can be considered as a phase annihilation point, which is of great significance for understanding the phase transition and thermodynamic stability of black holes.

On the other hand, we investigate the AdS black holes in canonical ensemble as topology thermodynamic defects in gravity's rainbow (for $p = \frac{3}{2}$). By substituting the mass (16) and entropy (18) of the black hole into Eq. (6), the generalized free energy is

$$\mathcal{F} = \frac{3g_\varepsilon^2 r_+ + 8P\pi r^3 - \frac{4\times 2^{1/4} g_\varepsilon^3 Q^{3/2} \log[\frac{r_+}{\ell}]}{\sqrt{3}}}{6 f_\varepsilon g_\varepsilon^3} - \frac{\pi r_+^2}{g_\varepsilon^2 \tau}. \quad (27)$$

The components of the vector field ϕ by Eq. (7) are

$$\phi^{r_+} = \frac{3g_\varepsilon^2 - \frac{4\times 2^{1/4} g_\varepsilon^3 Q^{3/2}}{\sqrt{3} r_+} + 24P\pi r_+^2}{6 f_\varepsilon g_\varepsilon^3} - \frac{2\pi r_+}{g_\varepsilon^2 \tau}, \quad (28)$$

$$\phi^{\Theta} = -\cot\Theta \csc\Theta.$$

To further investigate the thermodynamic behavior of the zero points, we obtain the expression for the corresponding zero points of τ by setting $\phi^{r_+} = 0$, as follows

$$\tau = \frac{36 f_\varepsilon g_\varepsilon \pi r_+^2}{-4\times 2^{1/4}\sqrt[3]{3}_\varepsilon Q^{3/2} + 9g_\varepsilon^2 r_+ + 72P\pi r_+^3}. \quad (29)$$

In Fig. 3a, we observe that there are three different types of black holes, and each category of black hole corresponds to different parameter space regions. We note that the branch $\tau < \tau_a$ corresponds to the small black hole region, and the branch $\tau > \tau_b$ corresponds to the large black hole region. Through calculation, we find that the winding number of the small and large black hole branches is $\omega = +1$. The middle black hole branch is located in the region of $\tau_a < \tau < \tau_b$, and for any zero points located on this branch, the number of winding is $\omega = -1$. Therefore, the total topology number is $W = +1 + (-1) + 1 = +1$. In addition, the large and small branches of black holes with the winding number of $+1$ represent thermodynamic stability, while the middle black hole branch with a winding number of -1 represents thermodynamic instability. The stability characteristics of black holes can also be analyzed from their positive and negative heat capacities. We identify the generation point

at $\tau/r_0 = \tau_a/r_0 = 42.9946$ and the annihilation point at $\tau/r_0 = \tau_b/r_0 = 47.8235$.

To calculate the topological charge of the black hole for the case $p = \frac{3}{2}$, we select choosing a random value of τ to determine the zero point of the vector field ($\tau/r_0 = 40$) in Fig. 3b, we observe one zero point $ZP_1(11.2188, \pi/2)$ of the unit vector field. According to the topological theory described in the preceding section, the winding number corresponding to this zero point is $\omega = +1$. For $\tau/r_0 = 45$, we can observe three critical points: $ZP_2(1.75418, \pi/2)$, $ZP_3(3.29013, \pi/2)$, and $ZP_4(8.40013, \pi/2)$ in Fig. 3c, corresponding to the winding numbers of $+1$, -1, and $+1$, respectively. At the ratio $\tau/r_0 = 50$ in Fig. 3d, the zero point $ZP_5(1.50618, \pi/2)$ has a positive winding number of $+1$.

For the pressure $Pr_0^2 = 0.1$, which exceeds the critical pressure P_c, there is only one single black hole branch in Fig. 4a, which is different from Fig. 3d, and the winding number of this branch is $+1$, so the topological number is $W = +1$. Due to the monotonically decreasing curve of τ, no generation or annihilation points don't exist. By fixing $\tau/r_0 = 5$, we have plotted the unit vector diagram associated with the zero point on this branch in Fig. 4b. The zero point is located at $(1.15625, \pi/2)$, and its corresponding topological number is $+1$. Furthermore, using the same the method, we find that no matter how the rainbow function parameters (f_ε and g_ε) change, the topological number of the black hole always remains at $+1$.

4.2 Case 2: $\frac{1}{2} < p < \frac{3}{2}$

As above, we can obtain the temperature function for $\frac{1}{2} < p < \frac{3}{2}$ is

$$T = \frac{g_\varepsilon^2 - 2^{-p} p (\frac{g_\varepsilon^2 Q}{p})^{\frac{2p}{2p-1}} r_+^{\frac{2}{1-2p}}}{2 f_\varepsilon g_\varepsilon \pi r_+}. \tag{30}$$

The potential function Φ and the components of vector field ϕ are

$$\Phi = \frac{(g_\varepsilon^2 - 2^{-p} p (\frac{g_\varepsilon^2 Q}{p})^{\frac{2p}{-1+2p}} r_+^{\frac{2}{1-2p}}) \csc\theta}{2 f_\varepsilon g_\varepsilon \pi r_+}, \tag{31}$$

$$\phi^{r+} = \frac{2^{-1-p} g_\varepsilon (2^p (2p-1) + (1+2p) Q (\frac{g_\varepsilon^2 Q}{p})^{\frac{1}{-1+2p}} r_+^{\frac{2}{1-2p}}) \csc\theta}{(2p-1) f_\varepsilon \pi r_+^2}, \tag{32}$$

$$\phi^\theta = -\frac{(g_\varepsilon^2 - 2^{-p} p (\frac{g_\varepsilon^2 Q}{p})^{\frac{2p}{-1+2p}} r_+^{\frac{2}{1-2p}}) \cot\theta \csc\theta}{2 f_\varepsilon g_\varepsilon \pi r_+}.$$

In Fig. 5a, the topological behavior exhibits a critical point CP_2 $(1.73139, \pi/2)$, which is similar to the case of $p = \frac{3}{2}$ in the canonical ensemble. When $\vartheta = 2\pi$ in Fig. 5b, the deflection angle of the vector field is -2π, so the topological charge of this critical point is -1, which is also a conventional critical point. The critical point corresponding to equation of state (17) is

$$\begin{aligned}
r_c &= \Big(\frac{2^{\frac{p}{2}-2p^2} \sqrt{p} \sqrt{1+2p} (\frac{g_\varepsilon^2 Q}{p})^{\frac{p}{2p-1}}}{g_\varepsilon \sqrt{2p-1}} \Big)^{2p-1}, \\
P_c &= \frac{1}{16\pi} \Big(\frac{2^{\frac{-p}{2}} p^{\frac{3}{2}} (\frac{g_\varepsilon^2 Q}{p})^{\frac{p}{2p-1}}}{g_\varepsilon \sqrt{1 - \frac{2}{1+2p}}} \Big)^{2-4p} \\
&\quad \times \Big(2g_\varepsilon^2 - 2^{\frac{3p}{2}} (1+2p) \Big(\frac{g_\varepsilon^2 Q}{p} \Big)^{\frac{2p}{2p-1}} \Big(\frac{\sqrt{p} \Big(\frac{g_\varepsilon^2 Q}{p} \Big)^{\frac{p}{2p-1}}}{g_\varepsilon \sqrt{1 - \frac{2}{1+2p}}} \Big)^{-2} \Big), \\
T_c &= \frac{1}{2 f_\varepsilon g_\varepsilon \pi} \Big(\frac{2^{\frac{-p}{2}} \sqrt{p} \Big(\frac{g_\varepsilon^2 Q}{p} \Big)^{\frac{p}{2p-1}}}{g_\varepsilon \sqrt{1 - \frac{2}{1+2p}}} \Big)^{1-2p} \\
&\quad \times \left(-2^{-p} p \Big(\frac{g_\varepsilon^2 Q}{p} \Big)^{\frac{2p}{2p-1}} + g_\varepsilon^2 \Big(\frac{2^{\frac{-p}{2}} \sqrt{p} \Big(\frac{g_\varepsilon^2 Q}{p} \Big)^{\frac{p}{2p-1}}}{g_\varepsilon \sqrt{1 - \frac{2}{1+2p}}} \Big)^2 \right).
\end{aligned} \tag{33}$$

Figure 5c shows the isobaric curves around the critical point CP_2 for the $\frac{1}{2} < p < \frac{3}{2}$, which is consistent with the case of $p = \frac{3}{2}$. The critical point CP_2 is the phase annihilation point.

On the other way, we consider the black hole solution as topological thermodynamic defects. The generalized free energy is

$$\mathcal{F} = \frac{-r_+}{2 f_\varepsilon g_\varepsilon} \Big(\frac{2^{-1-p} (1-2p)^2 (\frac{g_\varepsilon^2 Q}{p})^{\frac{2p}{2p-1}} r_+^{\frac{2}{1-2p}}}{g_\varepsilon^2 (-3+2p)} - \frac{8 P \pi r_+^2}{3 g_\varepsilon^2} - 1 \Big) - \frac{\pi r_+^2}{g_\varepsilon^2 \tau}. \tag{34}$$

The components of vector field ϕ are

$$\begin{aligned}
\phi^{r+} &= \frac{-8 f_\varepsilon g_\varepsilon \pi r_+ + (2g_\varepsilon^2 + 16 P \pi r_+^2 + 2^{-p} (1-2p) \Big(\frac{g_\varepsilon^2 Q}{p} \Big)^{\frac{2p}{2p-1}} r_+^{\frac{2}{1-2p}}) \tau}{4 f_\varepsilon g_\varepsilon^3 \tau}, \\
\phi^\Theta &= -\cot\Theta \csc\Theta.
\end{aligned} \tag{35}$$

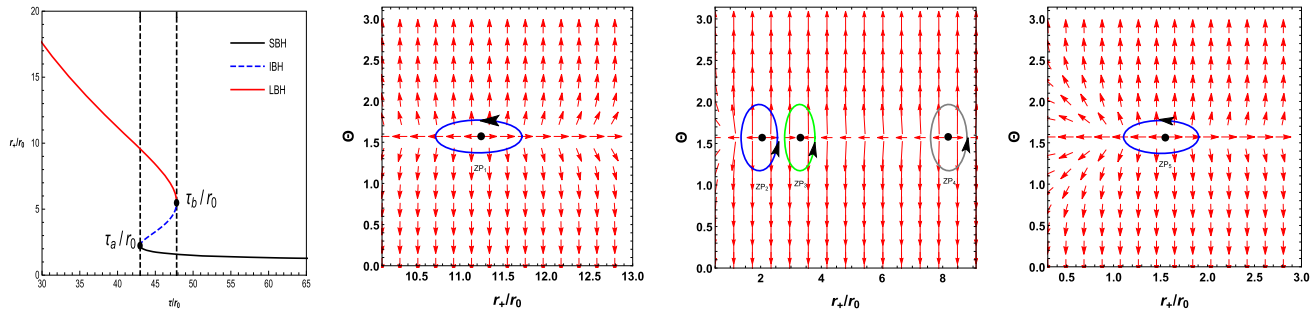

(a) (b) $\tau/r_0 = 40$ (c) $\tau/r_0 = 45$ (d) $\tau/r_0 = 50$

Fig. 3 Plot of unit vector n and zero points of ϕ^{r+} in canonical ensemble for $P < P_c$. **a–c** Unit vector n is shown in the r_+ vs θ plane and the black dots represent the zero points. **d** is the zero points of ϕ^{r+} in τ/r_0 vs r/r_0 plane. (By fixed $Pr_0^2 = 0.001$, $Q/r_0 = 1$, $f_\varepsilon/r_0 = 1.1$ and $g_\varepsilon/r_0 = 1.1$)

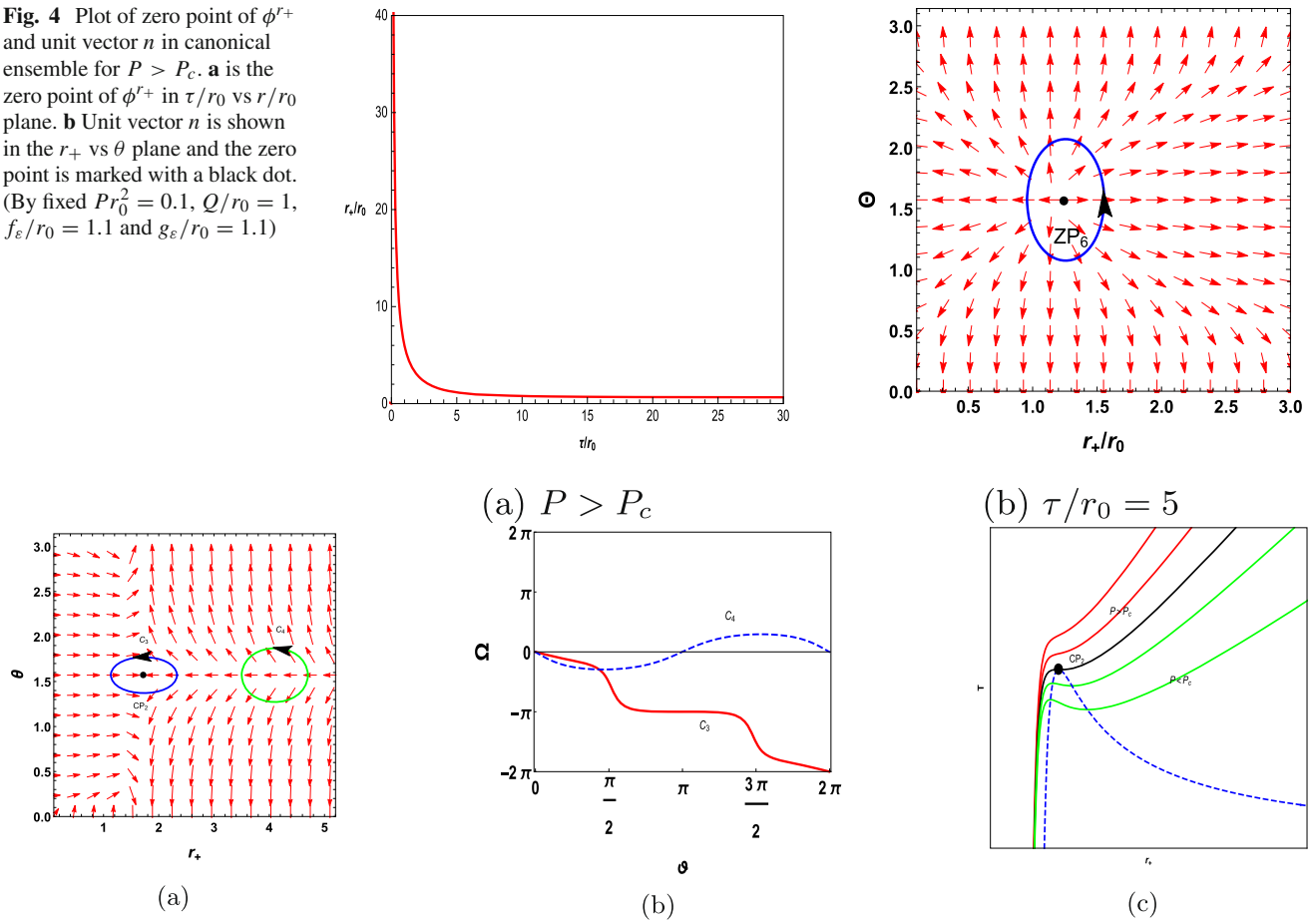

(a) $P > P_c$ (b) $\tau/r_0 = 5$

(a) (b) (c)

Fig. 4 Plot of zero point of ϕ^{r+} and unit vector n in canonical ensemble for $P > P_c$. **a** is the zero point of ϕ^{r+} in τ/r_0 vs r/r_0 plane. **b** Unit vector n is shown in the r_+ vs θ plane and the zero point is marked with a black dot. (By fixed $Pr_0^2 = 0.1$, $Q/r_0 = 1$, $f_\varepsilon/r_0 = 1.1$ and $g_\varepsilon/r_0 = 1.1$)

Fig. 5 **a** The normalized vector field n in the r_+ vs θ plane with the critical point CP_2 indicated by a black dot in canonical ensemble for $\frac{1}{2} < p < \frac{3}{2}$. **b** The deflection angle of the normalized vector field n in Ω vs ϑ plane for the contour C_3 and C_4. **c** Isobaric curves of AdS black hole at the critical point. (By fixed $Q = 1$, $f_\varepsilon = 1.1$ and $g_\varepsilon = 1.1$)

By solving Eq. (35) for $\phi^{r_+}=0$, the inverse of the equilibrium temperature is

$$**T=\begin{cases}\frac{g_\varepsilon}{4f_\varepsilon\pi r_+}\left(1+\frac{8P\pi r_+^2}{g_\varepsilon^2}-\frac{2\sqrt{2}g_\varepsilon\frac{f_\varepsilon^3U^3}{\log[\frac{r_+}{\ell}]^3}}{r_+}\right) & \text{for}\quad p=\frac{3}{2},\\ \frac{g_\varepsilon^2+8P\pi r_+^2+2^{\frac{3p-1}{1-2p}}(1-2p)r_+^{\frac{2}{1-2p}}\left(-\frac{f_\varepsilon g_\varepsilon(2p-3)r_+^{\frac{3-2p}{2p-1}}U}{2p-1}\right)^{2p}}{4f_\varepsilon g_\varepsilon\pi r_+} & \text{for}\quad \frac{1}{2}<p<\frac{3}{2},\end{cases}\tag{38}$$

$$M=\begin{cases}\frac{3g_\varepsilon^2r_++8P\pi r_+^3-6\sqrt{2}g_\varepsilon^3\frac{f_\varepsilon^3U^3}{\log[\frac{r_+}{\ell}]^2}}{6f_\varepsilon g_\varepsilon^3} & \text{for}\quad p=\frac{3}{2},\\ fracr_+\left(1+\frac{8P\pi r_+^2}{3g_\varepsilon^2}-2^{\frac{1-3p}{2p-1}}\frac{(3-2p)^{2p-1}}{g_\varepsilon^2(1-2p)^{2p-2}}r_+^{\frac{2}{1-2p}}(f_\varepsilon g_\varepsilon r_+^{\frac{3-2p}{2p-1}}U)^{2p}\right)2f_\varepsilon g_\varepsilon & \text{for}\quad \frac{1}{2}<p<\frac{3}{2}.\end{cases}\tag{39}$$

And the relevant thermodynamic quantities of AdS black holes are

$$\tau=\frac{8f_\varepsilon g_\varepsilon\pi r_+}{2g_\varepsilon^2+16P\pi r_+^2+2^{-p}(1-2p)\left(\frac{g_\varepsilon^2Q}{p}\right)^{\frac{2p}{2p-1}}r_+^{\frac{2}{1-2p}}}.\tag{36}$$

We have plotted the τ/r_0 vs r/r_0 diagram for two pressure cases, as shown in Fig. 6a and e. We can find that two situations: one with three black hole branches and another with black hole branch. The results are consistent with the previous case $p=\frac{3}{2}$. There is one generation and one annihilation points for $P<P_c$, and the generation/annihilation points don't exist for $P>P_c$. Each total topological number of black holes is $+1$. The precise position of each zero point in the vector diagram is as follows: $ZP_7(11.2436,\pi/2)$, $ZP_8(1.29884,\pi/2)$, $ZP_9(2.05961,\pi/2)$, $ZP_{10}(4.6527,\pi/2)$, $ZP_{11}(1.25628,\pi/2)$ and $ZP_{12}(1.26497,\pi/2)$, their winding numbers are $+1,+1,-1,+1,+1$ and $+1$, respectively. We also find that the topology of the black hole is not affected by the parameters f_ε and g_ε for this case. The influence of charge value on the topology of black holes is similar to the effect of pressure.

5 AdS black holes in rainbow gravity with nonlinear source in grand canonical ensemble

In this section, we mainly explore the topology of AdS black holes in rainbow gravity in grand canonical ensemble for two different regions p. The invariant electric potential of black hole can be expressed as

$$U=\begin{cases}-\frac{q_\varepsilon}{f_\varepsilon g_\varepsilon}\ln\left(\frac{r_+}{\ell}\right) & \text{for}\quad p=\frac{3}{2},\\ -\frac{q_\varepsilon}{f_\varepsilon g_\varepsilon}\left(\frac{2p-1}{2p-3}\right)(r_+)^{\frac{2p-3}{2p-1}} & \text{for}\quad \frac{1}{2}<p<\frac{3}{2}.\end{cases}\tag{37}$$

5.1 Case 1: $p=\frac{3}{2}$

The temperature function for $p=\frac{3}{2}$ is

$$T=-\frac{g_\varepsilon\left(3\sqrt{2}f_\varepsilon^3g_\varepsilon U^3-r_+log\left[\frac{r_+}{\ell}\right]^4+3\sqrt{2}g_\varepsilon f_\varepsilon^3U^3log\left[\frac{r_+}{\ell}\right]\right)}{2f_\varepsilon\pi r_+^2log\left[\frac{r_+}{\ell}\right]^4},\tag{40}$$

and the potential function $\Phi=\frac{T}{\sin\theta}$ is

$$\Phi=\frac{g_\varepsilon\csc\theta\left(-3\sqrt{2}f_\varepsilon^3g_\varepsilon U^3+r_+log\left[\frac{r_+}{\ell}\right]^4-3\sqrt{2}g_\varepsilon f_\varepsilon^3U^3log\left[\frac{r_+}{\ell}\right]\right)}{2f_\varepsilon\pi r_+{}^2log\left[\frac{r_+}{\ell}\right]^4}.\tag{41}$$

The vector components of $\phi=\left(\phi^{r_+},\phi^\theta\right)$ are

$$\begin{aligned}\phi^{r_+}&=\frac{g_\varepsilon\csc\theta\left(-r_++3\sqrt{2}g_\varepsilon\frac{f_\varepsilon^3U^3}{\log[\frac{r_+}{\ell}]^5}(4+\log[\frac{r_+}{\ell}](5+2\log[\frac{r_+}{\ell}]))\right)}{2f_\varepsilon\pi r_+^3},\\ \phi^\theta&=\frac{g_\varepsilon\cot\theta\csc\theta(-3\sqrt{2}f_\varepsilon^3g_\varepsilon U^3+r_+log[\frac{r_+}{\ell}]^4-3\sqrt{2}g_\varepsilon f_\varepsilon^3U^3log[\frac{r_+}{\ell}])}{2f_\varepsilon\pi r_+^2log[\frac{r_+}{\ell}]^4}.\end{aligned}\tag{42}$$

On the following the procedure discussed in Sect. 4, we plot the normalized vector n in r_+ vs θ plane (see Fig. 7). Different from the canonical ensemble, we find that there are three critical points: $CP_3(0.00226461,\pi/2)$, $CP_4(0.362146,\pi/2)$, and $CP_5(2.99109,\pi/2)$ in Fig. 7a. And these critical points are enclosed within contours C_5, C_6 and C_7, respectively. The critical points CP_3 and CP_5 carry a negative topological charge -1, signifying a conventional critical point associated with a first-order phase transition. It is worth noting that CP_4 has a positive topological charge $+1$.

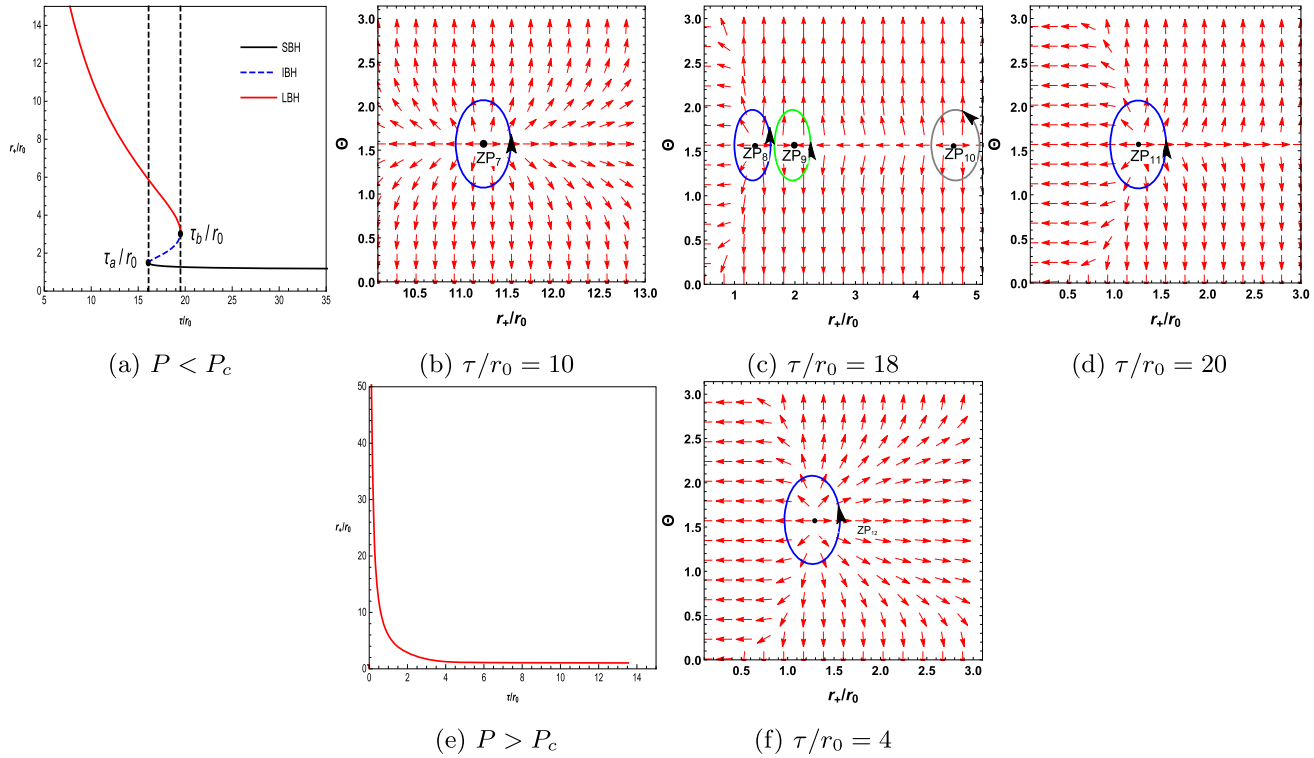

Fig. 6 Plot of zero points of ϕ^{r_+} in τ/r_0 vs r/r_0 plane and unit vector n in the θ vs r_+/r_0 plane in canonical ensemble for two pressure values. **a** and (*e*) are the zero points of ϕ^{r_+} in τ/r_0 vs r/r_0 plane. **b**–**d** and **f** are unit vector graphs, and the black dots represent the zero points (by fixed $Q/r_0 = 1$, $f_\varepsilon/r_0 = 1.1$ and $g_\varepsilon/r_0 = 1.1$)

When electric potential of black hole $U = 1.1$, our result shows that there is a critical point CP_6 (conventional critical point) with a topological charge of -1 which is consistent with the canonical ensemble (see Fig. 7c, d).

We plot the isobaric curves near the conventional critical point CP_5 and the novel critical point CP_4 in Fig. 8. By analyzing the critical topological structure of black holes, we find that the critical point CP_5 with negative topological charge corresponds exactly to the maximum critical temperature. We also observe the existence of an unstable region near the conventional critical point CP_5, which can be eliminated by Maxwell's area law. However, the novel critical point CP_4 with positive topological charge corresponds to the minimum critical temperature, and Maxwell's equal area law can not be applied near this point. Therefore, there is no first-order phase transition occurring near the novel critical point.

In the next step, we identify AdS black hole as topological thermodynamic defects, and the generalized free energy is

$$\begin{aligned}\mathcal{F} &= E - \frac{S}{\tau} - UQ \\ &= -\frac{\pi r_+^2}{g_\varepsilon^2 \tau} - \frac{3 f_\varepsilon^2 U^3}{\sqrt{2}\log[\frac{r_+}{\ell}]^2} \\ &\quad + \frac{3 g_\varepsilon^2 r_+ + 8P\pi {r_+}^3 - 6\sqrt{2} g_\varepsilon^3 \frac{f_\varepsilon^3 U^3}{\log[\frac{r_+}{\ell}]^2}}{6 f_\varepsilon g_\varepsilon^3}. \end{aligned} \tag{43}$$

The components of vector field ϕ are

$$\begin{aligned}\phi^{r_+} &= \frac{g_\varepsilon^2 \tau + 8P\pi {r_+}^2 \tau - 4 f_\varepsilon g_\varepsilon \pi r_+}{2 f_\varepsilon g_\varepsilon^3 \tau} + \frac{5\sqrt{2} f_\varepsilon^2 U^3}{r_+ \log[\frac{r_+}{\ell}]^3}, \\ \phi^{\Theta} &= -\cot\Theta \csc\Theta. \end{aligned} \tag{44}$$

By $\phi^{r_+} = 0$, we can derive

$$\tau = \frac{4 f_\varepsilon g_\varepsilon \pi\, r_+^2 log[\frac{r_+}{\ell}]^3}{10\sqrt{2} f_\varepsilon^3 g_\varepsilon^3 U^3 + r_+ (g_\varepsilon^2 + 8P\pi {r_+}^2) log[\frac{r_+}{\ell}]^3}. \tag{45}$$

The relationship between τ/r_0 and r_+/r_0 is shown in Fig. 9a. The plot exhibits two black hole branches for the region $\tau < \tau_c$ and $\tau > \tau_c$, which is different from the canonical ensemble. For the branch $\tau < \tau_c$ (the red dashed line) corresponds to the unstable region of the black hole with winding number -1. For the branch $\tau > \tau_c$ (the black solid line) represents the stable black hole region with winding number of $+1$. The annihilation point is situated at $\tau/r_0 = \tau_c/r_0 = 39.0111$. And we find two zero points ZP_{13} and ZP_{14} with the winding number -1 and $+1$ in Fig. 9b. As

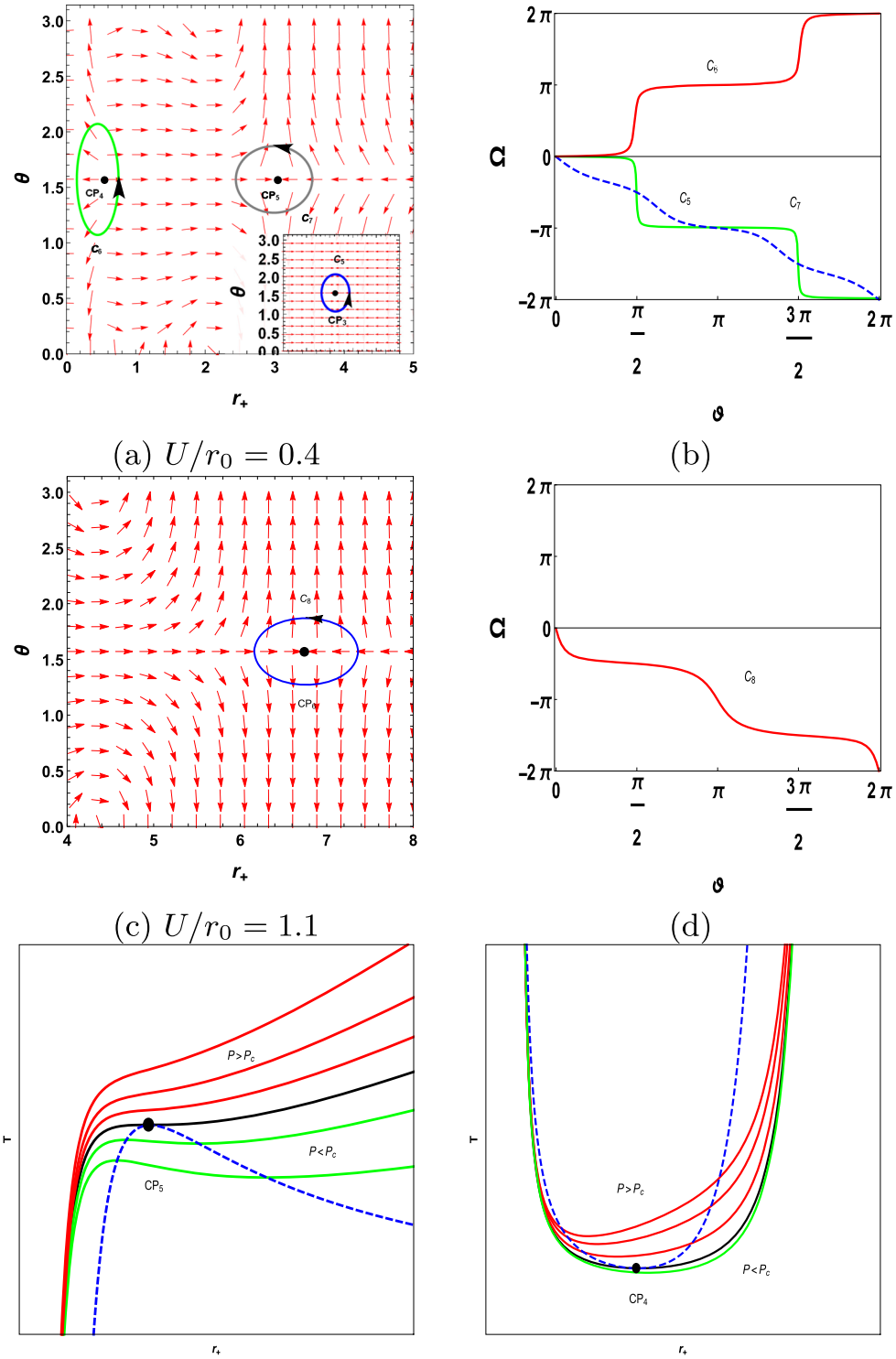

Fig. 7 **a** and **c** the normalized vector field n in the r_+ vs θ plane in grand canonical ensemble and the black dots represent the critical points for two potential values. **b** and **d** Ω vs ϑ plot for the contours C_5, C_6, C_7 and C_8. (By fixed $\ell = 1$, $f_\varepsilon = 1.1$ and $g_\varepsilon = 1.1$)

Fig. 8 The isobaric curves of AdS black hole near the critical points CP_4 and CP_5 in grand canonical ensemble

a result, the topology number of black holes in grand canonical ensemble is $W = 0$. It is worth noting that although the total topological number W is usually non-zero in canonical ensemble. This result is inconsistent with the observed results in canonical ensemble, which means that the ensemble has an impact on the AdS black hole topology.

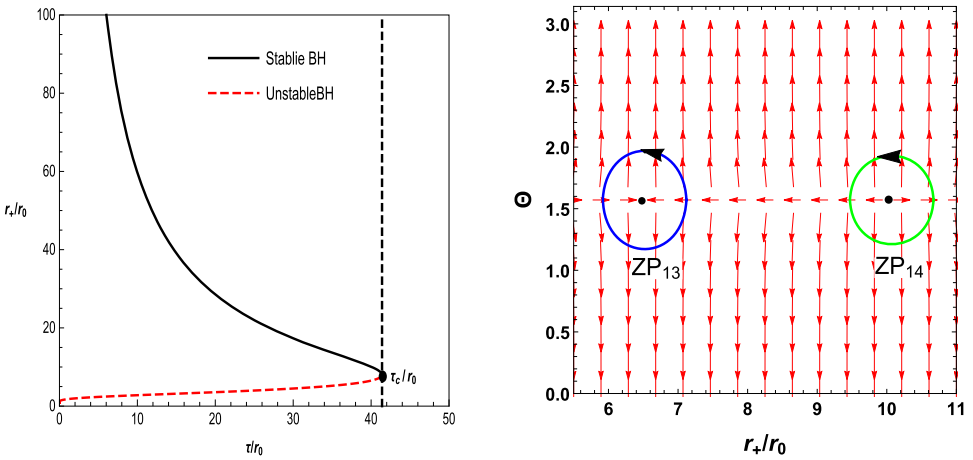

(a) (b) $\tau/r_0 = 40$

Fig. 9 Plot of zero points of ϕ^{r_+} and unit vector n in grand canonical ensemble. **a** Unit vector n is shown in the r_+ vs θ plane and the zero points are marked with black dots. **b** The zero points of ϕ^{r_+} in τ/r_0 vs r/r_0 plane. (By fixed $\ell = 1$, $U/r_0 = 0.4$, $f_\varepsilon/r_0 = 1.1$ and $g_\varepsilon/r_0 = 1.1$)

5.2 Case 2: $\frac{1}{2} < p < \frac{3}{2}$

The expression for the temperature function is

$$T = \frac{1}{8 f_\varepsilon g_\varepsilon \pi r_+}\left(4g_\varepsilon^2 - (2p^2-p) r_+^{\frac{2}{1-2p}} 2^{\frac{p-1}{2p-1}} \times \left(\frac{f_\varepsilon g_\varepsilon (3-2p) r_+^{\frac{3-2p}{2p-1}} U}{-1+2p}\right)^{2p}\right). \tag{46}$$

The potential function Φ is

$$\Phi = \frac{\csc\theta}{8 f_\varepsilon g_\varepsilon \pi r_+}\left(4g_\varepsilon^2 - (2p^2-p) r_+^{\frac{2}{1-2p}} 2^{\frac{p-1}{2p-1}} \times \left(\frac{f_\varepsilon g_\varepsilon (3-2p) r_+^{\frac{3-2p}{2p-1}} U}{-1+2p}\right)^{2p}\right), \tag{47}$$

and the vector field $\phi = \left(\phi^{r_+}, \phi^\theta\right)$ with

$$\begin{aligned}\phi^{r_+} &= \frac{-1}{4 f_\varepsilon g_\varepsilon \pi r_+^2}\left(2g_\varepsilon^2 - 2^{\frac{p-2p^2}{2p-1}} \frac{p(3-2p)^{2p}}{(1-2p)^{2p-2}} r_+^{\frac{4p^2-6p+2}{1-2p}} \times (f_\varepsilon g_\varepsilon U)^{2p} \csc\theta\right),\\ \phi^\theta &= \frac{-\cot\theta\csc\theta}{8 f_\varepsilon g_\varepsilon \pi r_+}\left(4g_\varepsilon^2 - (2p^2-p) r^{\frac{2}{1-2p}} 2^{\frac{p-1}{2p-1}} \times \left(\frac{f_\varepsilon g_\varepsilon (3-2p) r_+^{\frac{3-2p}{2p-1}} U}{-1+2p}\right)^{2p}\right).\end{aligned} \tag{48}$$

We have observed that there is a critical point CP_6 (a phase annihilation point) included in the contour C_9, while the contour C_{10} does not contain critical point.

Consequently, at $\vartheta = 2\pi$, the total topological charge is -1 (see Fig. 10).

Furthermore, we can interpret the black hole solutions as defects within the topological thermodynamics framework. The generalized free energy can be expressed as

$$\begin{aligned}\mathcal{F} &= E - \frac{S}{\tau} - UQ\\ &= \frac{r_+ + \frac{8P\pi r_+^3}{3g_\varepsilon^2} - \frac{2^{\frac{1-3p}{2p-1}}(3-2p)^{2p-1}}{g_\varepsilon^2(1-2p)^{2p-2}} r_+^{\frac{3-2p}{1-2p}} (U f_\varepsilon g_\varepsilon r_+^{\frac{3-2p}{2p-1}})^{2p}}{2 f_\varepsilon g_\varepsilon}\\ &\quad - \frac{\pi r^2}{g_\varepsilon^2 \tau} - \frac{2^{p-1} p U^{2p} r_+^{3-2p} (\frac{f_\varepsilon g_\varepsilon (3-2p)}{2p-1})^{2p-1}}{g_\varepsilon^2},\end{aligned} \tag{49}$$

and the components of vector field ϕ are

$$\begin{aligned}\phi^{r_+} &= \frac{1}{2 f_\varepsilon g_\varepsilon} - \frac{2\pi r_+}{g_\varepsilon^2} + \frac{4P\pi r_+^2}{f_\varepsilon g_\varepsilon^3}\\ &\quad + \frac{2^p (f_\varepsilon g_\varepsilon (3-2p) r_+^{\frac{3-2p}{2p-1}} U)^{2p}}{4 f_\varepsilon g_\varepsilon^3} r_+^{\frac{2}{1-2p}} \left(\frac{-2p}{(2p-1)^{2p-1}} + \frac{2^{\frac{-2p^2}{2p-1}}}{(2p-1)^{2p-2}}\right),\\ \phi^\Theta &= -\cot\Theta\csc\Theta.\end{aligned} \tag{50}$$

By solving $\phi^{r_+} = 0$, we derive

$$\tau = \frac{8 f_\varepsilon g_\varepsilon \pi r_+}{2g_\varepsilon^2 + 16\pi r_+^2 + 2^p r_+^{\frac{6p-4p^2-2}{2p-1}} f_\varepsilon^{2p} g_\varepsilon^{2p} U^{2p} (3-2p)^{2p} \left(\frac{-2p}{(2p-1)^{2p-1}} + \frac{2^{\frac{-2p^2}{2p-1}}}{(2p-1)^{2p-2}}\right)}. \tag{51}$$

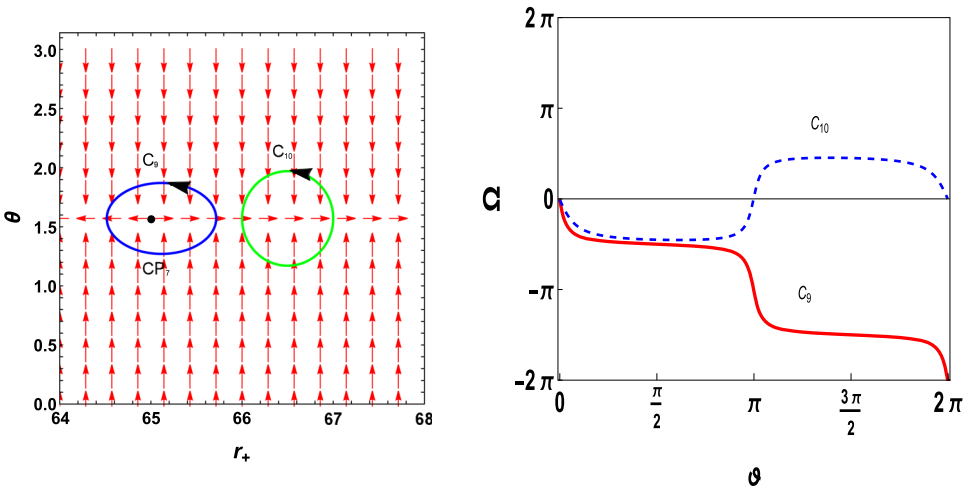

(a) (b)

Fig. 10 Left: the normalized vector field n in the r_+ vs θ plane with a critical point indicated by a black dot in grand canonical ensemble. Right: plot of Ω vs ϑ for the contours C_9 and C_{10}. (By fixed $U = 1.5$, $f_\varepsilon = 1.1$ and $g_\varepsilon = 1.1$)

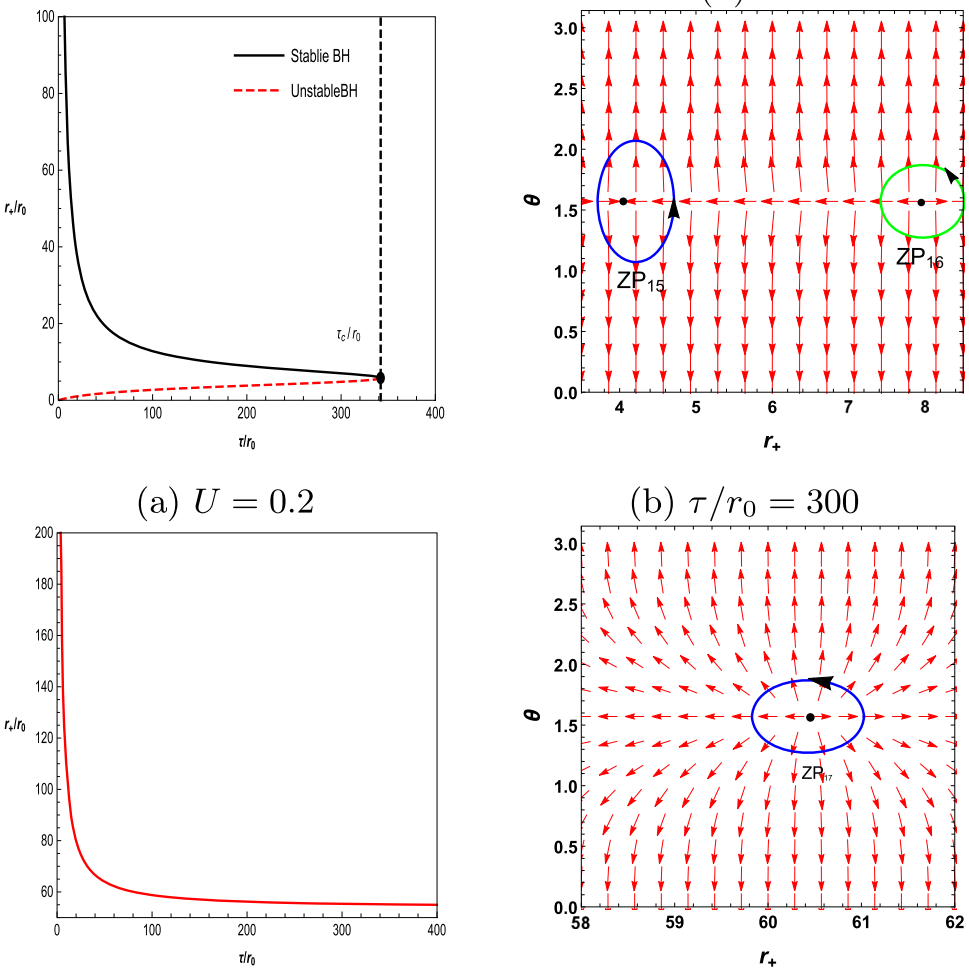

(a) $U = 0.2$ (b) $\tau/r_0 = 300$

(c) $U = 1$ (d) $\tau/r_0 = 100$

Fig. 11 **a** and **c** The zero points of ϕ^{r+} in τ/r_0 vs r_+/r_0 for black holes in grand canonical ensemble for two potential values. **b** and **d** The Unit vector field n in the r_+/r_0 vs Θ plane with zero points indicated by black dots (By fixed $f_\varepsilon/r_0 = 1.1$, $g_\varepsilon/r_0 = 1.1$ and $Pr_0^2 = 0.001$)

Table 1 Topological number W, the number of generation and annihilation points of various black holes in the canonical ensemble and the grand canonical ensemble

Ensembles	Black holes	Topological charge W	Generation point	Annihilation point
	AdS BH with $p = \frac{3}{2}$ in rainbow gravity	$+1$	1 or 0	1 or 0
	AdS BH with $\frac{1}{2} < p < \frac{3}{2}$ in rainbow gravity	$+1$	1 or 0	1 or 0
	Phantom AdS BH in massive gravity [78]	$+1$	1 or 0	1 or 0
CE	4D dyonic AdS BH [79]	$+1$	1 or 0	1 or 0
	4D Euler-Heisenberg-AdS BH [80]	$+1$ or 0	0 or 1	1 or 0
	charged dilatonic BH [81]	$+1$ or 0	0 or 1	0
	AdS BH with $p = \frac{3}{2}$ in rainbow gravity	0	0	1
	AdS BH with $\frac{1}{2} < p < \frac{3}{2}$ in rainbow gravity	$+1$ or 0	0	0 or 1
	Phantom AdS BH in massive gravity [78]	$+1$ or 0	0 or 1	0
GCE	4D dyonic AdS BH [79]	$+1$ or 0	0 or 1	0
	4D Euler–Heisenberg-AdS BH [80]	0	1 or 0	1 or 0
	Charged dilatonic BH [81]	$+1$ or 0	0 or 1	0 or 1

We obtain two black hole branches (stable and unstable) with a total topological number $-1 + (+1) = 0$ as shown in Fig. 11a. Additionally, there is one annihilation point located at $\tau/r_0 = \tau_c/r_0 = 342.008$, which is consistent with the description of the case of $p = \frac{3}{2}$ in the grand canonical ensemble. In Fig. 11b, we have identified two zero points ZP_{15} and ZP_{16} with winding numbers of -1 and $+1$, respectively. With increasing the electric potential to $U = 1$, there is a single black hole branch with winding number of $+1$ at $(0.362146, \pi/2)$ (see Fig. 11c, d). Furthermore, we also find that the pressure value has no effect on the topology of the black hole in the grand canonical ensemble.

A comparison for different black hole cases in Table 1, we have compared the topological charges and the number of generation/annihilation points of the AdS black holes with nonlinear parameter in rainbow gravity ($p = \frac{3}{2}$ and $\frac{1}{2} < p < \frac{3}{2}$) with other black holes in the canonical ensemble and the grand canonical ensemble. From the table, we can see that the AdS black holes with nonlinear parameter in rainbow gravity can be classified into the same topological class as the phantom black hole under massive gravity and the 4D dynamic AdS black hole in the canonical ensemble. In the grand canonical ensemble, the AdS black hole with $p = \frac{3}{2}$ in rainbow gravity and 4D black holes have the same topological charge $W = 0$. The AdS black hole with $\frac{1}{2} < p < \frac{3}{2}$ in rainbow gravity and charged expanding black holes, phantom black holes under massive gravity, and 4D dynamic AdS black holes have the same topological charge $W = +1$ or 0. However, the difference between the AdS black hole under rainbow gravity and other black holes is that there is no generation point in the τ vs r image of the black hole in the grand canonical ensemble.

6 Conclusion

In this paper, we have delved into exploring the thermodynamic topology of a four-dimensional AdS black hole with nonlinear source in the canonical ensemble and the grand canonical ensemble under the rainbow gravity framework. We have observed that both types of black holes ($p = \frac{3}{2}$ and $\frac{1}{2} < p < \frac{3}{2}$) in the two ensembles have a topological charge -1, but in grand canonical ensemble, for black holes with $p = \frac{3}{2}$, a novel critical point appears beside the conventional critical point. By calculating the winding number at the defects, we have found that: in canonical ensemble, the topological number of both types of black holes is $+1$, we can observe one generation and one annihilation point or no generation/annihilation for the specific pressure value. In the grand canonical ensemble, the topological number of black holes for $p = \frac{3}{2}$ is 0 with one annihilation point. The topological number of black holes for $\frac{1}{2} < p < \frac{3}{2}$ can be 0 and $+1$, and there may be one annihilation point or absence of generation/annihilation depending on the electric potential value. Based on the above analysis, we have concluded that these two types of black holes belong to the same topological class in canonical ensemble, but belong to different topological classes in grand canonical ensemble. In other words, the topological classification of black holes is influenced by the choice of ensemble, the system pressure and the electric potential. In addition, we have found that the topological charge of black holes remains independent of the rainbow function parameters f_ε and g_ε, which indicates that the rainbow gravitational effect alters the thermodynamic properties of black holes, but does not impact on topological charges.

Acknowledgements This work is supported by the National Science Foundation of China under Grant Nos. 12373022, U1731107.

Data Availability Statement My manuscript has no associated data. [Authors' comment: The paper is purely theoretical and thus does not yield associated experiment data.]

Code Availability Statement My manuscript has no associated code/software. [Author's comment: Code/Software sharing not applicable to this article as no code/software was generated or analyzed during the current study.]

Funded by SCOAP[3].

References

1. J.D. Bekenstein, Phys. Rev. D **7**, 2333 (1973)
2. J.D. Bekenstein, Lettere al Nuovo Cimento **4**, 737 (1972)
3. J.D. Bekenstein, Phys. Rev. D **7**, 949 (1973)
4. S.W. Hawking, Commun. Math. Phys. **43**, 199 (1975)
5. S.W. Hawking, Phys. Rev. D. **30**, 248 (1974)
6. J.D. Bekenstein, Phys. Rev. D. **9**, 3292 (1974)
7. J.D. Bekenstein, Phys. Rev. D **12**, 3077 (1975)
8. S.W. Hawking, Phys. Rev. D **13**, 191 (1976)
9. P. Candelas, D.W. Sciama, Phys. Rev. Lett. **38**, 1372 (1977)
10. R.M. Wald, Phys. Rev. D **20**, 1271 (1979)
11. J.M. Bardeen, B. Carter, S.W. Hawking, Commun. Math. Phys. **31**, 161 (1973)
12. Y. Ladghami, T. Ouali, Phys. Dark Universe **44**, 101471 (2024)
13. S.W. Hawking, D.N. Page, Commun. Math. Phys. **87**, 577 (1983)
14. E. Witten, Theor. Math. Phys. **2**, 253 (1998)
15. A. Chamblin, R. Emparan, C.V. Johnson, R.C. Myers, Phys. Rev. D **60**, 064018 (1999)
16. A. Chamblin et al., Phys. Rev. D **60**, 104026 (1999)
17. D. Kubizňák, R.B. Mann, JHEP **07**, 033 (2012)
18. N. Altamirano, D. Kubizňák, R.B. Mann, Phys. Rev. D **60**, 101502 (2013)
19. A.M. Frassino, D. Kubizňák, R.B. Mann, JHEP **09**, 080 (2014)
20. D.C. Zou, R. Yue, M. Zhang, Eur. Phys. J. C **77**, 256 (2017)
21. S.W. Wei, Y.X. Liu, Phys. Rev. D **90**, 044057 (2014)
22. A. Dehyadegari, A. Sheykhi, A. Montakhab, Phys. Rev. D **96**, 084012 (2017)
23. Z. Dayyani, A. Sheykhi, Phys. Rev. D **98**, 104026 (2018)
24. A. Dehyadegari, A. Sheykhi, A. Montakhab, Phys. Lett. B **768**, 235 (2017)
25. A. Dehyadegari, B.R. Majhi, A. Sheykhi, Phys. Lett. B **791**, 30 (2019)
26. P. Wang, H. Wu, H. Yang, J. Cosmol. Astropart. Phys. **04**, 052 (2019)
27. G. Guo, P. Wang, H. Wu, H. Yang, Phys. Rev. D **105**, 064069 (2022)
28. Y. Sekhmani, J. Rayimbaev, G.G. Luciano, R. Myrzakulov, D.J. Gogoi, Phys. Dark Universe **84**, 277 (2024)
29. R.H. Ali, G. Abbas, G. Mustafa, Phys. Dark Universe **44**, 101465 (2024)
30. G. Amelino-Camelia, J.R. Ellis, N.E. Mavromatos, D.V. Nanopoulos, Int. J. Mod. Phys. A **12**, 607 (1997)
31. D. Amati, M. Ciafaloni, G. Veneziano, Phys. Lett. B **41**, 216 (1989)
32. G. Amelino-Camelia, J.R. Ellis, N.E. Mavromatos, D.V. Nanopoulos, Int. J. Mod. Phys. A **393**, 763 (1998)
33. G. Amelino-Camelia, Int. J. Mod. Phys. D **11**, 35 (2002)
34. J. Magueijo, L. Smolin, Phys. Lett. B **88**, 190403 (2002)
35. G. Amelino-Camelia, (2002) arXiv preprint arXiv:gr-qc/0207049
36. F. Girelli, E.R. Livine, D. Oriti, Nucl. Phys. B **708**, 411 (2005)
37. G. Amelino-Camelia, (2008) arXiv:0806.0339
38. L. Smolin, Nucl. Phys. B **742**, 142 (2006)
39. G. Amelino-Camelia, Phys. Lett. B **528**, 181 (2002)
40. G. Amelino-Camelia, Int. J. Mod. Phys. D **11**, 35 (2002)
41. G. Amelino-Camelia, Phys. Lett. B **418**, 34 (2002)
42. J. Magueijo, L. Smolin, Phys. Rev. D **67**, 044017 (2003)
43. A. Haldar, R. Biswas, Gen. Relativ. Gravit. **51**, 72 (2019)
44. M. Dehghani, Phys. Lett. B **785**, 274 (2018)
45. J. Magueijo, L. Smolin, Class. Quantum Gravity **21**, 1725 (2004)
46. P. Li, M. He, J.C. Ding, X.R. Hu, J.B. Deng, Adv. High Energy. Phys. **2018**, 1043639 (2018)
47. S.W. Wei, Y.X. Liu, Phys. Rev. D **105**, 104003 (2022)
48. S.W. Wei, Y.X. Liu, R.B. Mann, Phys. Rev. Lett. **129**, 191101 (2022)
49. Y.S. Duan, SLAC-PUB-3301 (1984)
50. Y.S. Duan, M.L. Ge, Sci. Sin. **9**, 1072 (1979)
51. J. Sadeghi, M.A.S. Afshar, S.N. Gashti, M.R. Alipour, Phys. Scr. **99**, 025003 (2024)
52. N.C. Bai, L. Li, J. Tao, Phys. Rev. D **107**, 064015 (2023)
53. N.J. Gogoi, P. Phukon, Phys. Rev. D **107**, 106009 (2023)
54. J. Sadeghi, S.N. Gashti, M.R. Alipour, M.A.S. Afshar, Chin. Phys. C **48**, 115115 (2024)
55. A. Mehmood, M.U. Shahzad, (2023) arXiv:2310.09907
56. M. Rizwan, K. Jusufi, Eur. Phys. J. C **83**, 944 (2023)
57. S.P. Wu, S.W. Wei, Phys. Rev. D **110**, 024054 (2024)
58. B. Hazarika, B.E. Panah, P. Phukon, Eur. Phys. J. C **84**, 1 (2024)
59. J. Sadeghi, S.N. Gashti, M.R. Alipour, M.A.S. Afshar, Ann. Phys. **455**, 169391 (2023)
60. P.K. Yerra, C. Bhamidipati, Phys. Rev. D **105**, 104053 (2022)
61. P.K. Yerra, C. Bhamidipati, Phys. Rev. D **106**, 064059 (2022)
62. S.W. Wei, Y.X. Liu, Phys. Rev. D **107**, 064006 (2023)
63. M.Y. Zhang, H. Chen, H. Hassanabadi et al., Eur. Phys. J. C **83**, 773 (2023)
64. D. Wu, Phys. Rev. D **107**, 024024 (2023)
65. D. Wu, S.Q. Wu, Phys. Rev. D **107**, 084002 (2023)
66. X.D. Zhu, D. Wu, D. Wen, Phys. Lett. B **856**, 138919 (2024)
67. Y. Du, X. Zhang, Eur. Phys. J. C **83**, 927 (2023)
68. M.Y. Zhang, H. Chen, H. Hassanabadi, Z.W. Long, H. Yang, Phys. Lett. B **856**, 138885 (2024)
69. Y. Du, H. Li, X. Zhang, Symmetry **16**, 1577 (2024)
70. B. E. Panah, B. Hazarika, P. Phukon, (2024) arXiv:2405.20022
71. Y. Sekhmani, S.N. Gashti, M.A.S. Afshar et al., (2024) arXiv:2409.04997
72. F. Simovic, D. Fusco, R.B. Mann, Phys. Lett. B **801**, 135191 (2020)
73. M.K. Zangeneh, M.H. Dehghani, A. Sheykhi, Phys. Rev. D **92**, 104035 (2015)
74. M. Dehghani, Phys. Rev. D **94**, 104071 (2016)
75. D. Kastor, S. Ray, J. Traschen et al., Class. Quantum Gravity **26**, 195011 (2009)
76. S. Gunasekaran, R.B. Mann, D. Kubiznak et al., JHEP **11**, 110 (2012)
77. D. Chen, G. Gingyu, J. Tao et al., Nucl. Phys. B **918**, 115 (2017)
78. H. Chen, D. Wu, M.Y. Zhang, H. Hassanabadi, Z.W. Long, Phys. Dark Universe **46**, 101617 (2024)
79. N.J. Gogoi, P. Phukon, Phys. Rev. D **108**, 066016 (2023)
80. N.J. Gogoi, P. Phukon, Phys. Dark Universe **44**, 101456 (2024)
81. B. Hazarika, B.E. Panah, P. Phukon, Eur. Phys. J. C **1**, 84 (2024)